

LEVERAGING BI-FOCAL PERSPECTIVES AND GRANULAR FEATURE INTEGRATION FOR ACCURATE RELIABLE EARLY ALZHEIMER'S DETECTION

SHRAVAN VENKATRAMAN¹, PANDIYARAJU V², ABESHEK A³, PAVAN KUMAR S⁴,
ARAVINTAKSHAN S A⁵

¹⁻⁵School of Computer Science and Engineering, Vellore Institute of Technology, Chennai, Tamil Nadu, India

(e-mails: {pandiyaraju.v@vit.ac.in, shravan.venkatraman18@gmail.com, abeshk.a@gmail.com, s.pavankumar2003@gmail.com, aravintcs176@gmail.com})

Corresponding author: Pandiyaraju V (e-mail: pandiyaraju.v@vit.ac.in)

ABSTRACT Being the most commonly known neurodegeneration, Alzheimer's Disease (AD) is annually diagnosed in millions of patients. The present medical scenario still finds the exact diagnosis and classification of AD through neuroimaging data as a challenging task. Traditional CNNs can extract a good amount of low-level information in an image while failing to extract high-level minuscule particles, which is a significant challenge in detecting AD from MRI scans. To overcome this, we propose a novel Granular Feature Integration method to combine information extraction at different scales along with an efficient information flow, enabling the model to capture both broad and fine-grained features simultaneously. We also propose a Bi-Focal Perspective mechanism to highlight the subtle neurofibrillary tangles and amyloid plaques in the MRI scans, ensuring that critical pathological markers are accurately identified. Our model achieved an F1-Score of 99.31%, precision of 99.24%, and recall of 99.51%. These scores prove that our model is significantly better than the state-of-the-art (SOTA) CNNs in existence.

INDEX TERMS Alzheimer's Disease, Bi-Focal Perspectives, Deep Learning, Granular Feature Integration

I. INTRODUCTION

CHARACTERIZED by chronic neurodegeneration, Alzheimer's disease causes systematic brain neuron deterioration. It affects the cognitive abilities as well as reduces the individual's ability to perform simple tasks thereby turning out to be the biggest cause of dementia in older people [1]. An individual diagnosed with AD suffers from memory loss, problems in speaking, inability to understand, etc. Apart from these symptoms, AD also results in the formation of abnormal masses (amyloid plaques) and knotted strings of fibers known as neurofibrillary tangles of the brain. Furthermore, disconnection of neurons is observed as well constituting to the hallmark features of AD [2]. The disease primarily targets regions of the brain responsible for cognition, memory, and communication. The hippocampus and the entorhinal cortex of the brain, known for their responsibility to create a memory, are among the earliest to be targeted. The underlying cause of AD remains is still not well known, it is speculated that it might be an amalgamation of genetic factors along with lifestyle and environmental conditions.

Age is considered to be the primary risk factor since majority of positive cases are recorded in patients aged over 65 years. Genetics play a crucial role, since a family history of AD also increases the risk. Diagnosis of AD is a tedious task involving exhaustive procedures like evaluating the family history, physical examination, cognitive and neurological tests. MRI scans with doctors' assistance are given great importance to diagnose AD. These MRI scans provide an accurate image of the brain including the description of their shape and size. Comparing them with the history of the patient, memory decline and other cognitive functions are considered to be the primary symptoms of dementia [3]. In this work, we aim to contribute to the advancing AD detection by development of a state-of-the-art mechanism through our proposed method, thereby efficiently improving the quality of medical diagnosis by adopting Deep Learning (DL) algorithms.

Complex DL algorithms have a major influence in detecting AD due to their capability to analyse wide range of data. But the underlying reason for utilization of DL algorithms is

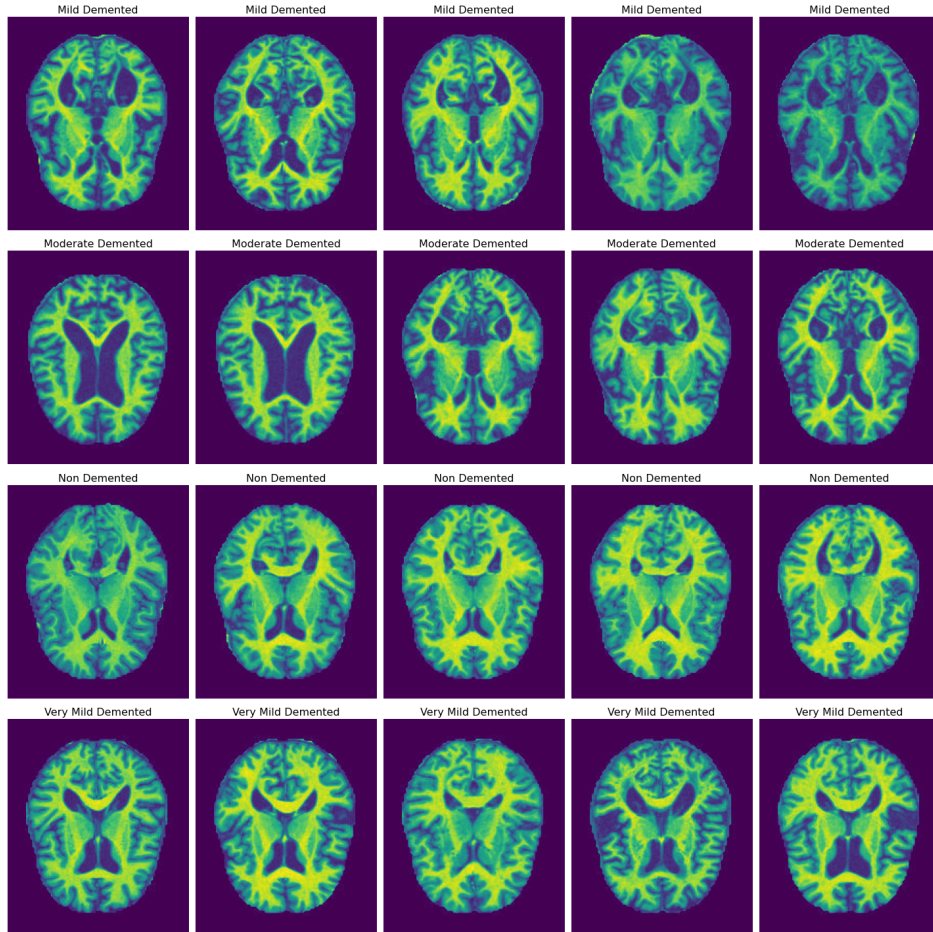


FIGURE 1. Sample Images of MRI Scans from the OASIS Dataset Representing Each Class of AD

because of its ability to process and interpret MRI scans to identify patterns of brain degeneration. Convolutional Neural Networks (CNNs), in particular can recognize such intricate patterns in image data which in association with advanced algorithms enable early diagnosis of AD and contribute in assisting with slowing down its progression towards dementia [4]. DL models provide an automatic analysis of MRI scans from patients, improving diagnostic efficiency while yielding promising results in AD identification [5].

The DL model, BFPCNN, introduced in this research article, utilizes Bi-Focal Perspectives and integrates Granular Features for robust extraction of high-level and low-level features to help healthcare professionals to assist healthcare professionals to identify abnormalities in the brain in an efficient manner while consuming lesser duration at the same time. We utilized the open-access series of imaging studies, OASIS-1 dataset [6], which includes cross-sectional MRI data acquired from nondemented young, demented older adults, and the middle-aged. Sample images from each class of the dataset is shown in Figure 1. Our research is then compared with that previously conducted and other high-performance CNN models. Consequently, our results show that our model outperforms previous works along with SOTA

CNNs, highly accurately extracting features and classifying the MRI scans.

The contributions of this research are as follows:

- Granular Feature Integration for Multi-Scale Feature Extraction:** The proposed BFPCNN introduces a Granular Feature Integration mechanism, effectively addressing the limitations of traditional CNNs that struggle to extract fine-grained, high-level details necessary for Alzheimer's diagnosis. This method ensures that the model captures both broad structural patterns and fine-grained pathological markers, such as subtle brain abnormalities, overcoming the traditional trade-off between local and global feature extraction.
- Bi-Focal Perspective Mechanism in BFPCNN for Highlighting Key Biomarkers:** The proposed Bi-Focal Perspective mechanism specifically enhances the identification of critical Alzheimer's biomarkers, such as neurofibrillary tangles and amyloid plaques, which are often missed by conventional models. By focusing on these subtle features, the proposed model directly addresses the challenge of detecting intricate pathological indicators in MRI scans, improving diagnostic precision.

II. RELATED WORKS

Helaly et al. [7] showcase the potential of deep learning, CNNs, in the early-stage detection of AD via biomedical images. Their study is based on multi-class as well as binary classification in order to classify between different stages of AD; it supports proper diagnosis and further treatment plan. They enhance the detection with sparse data by fine-tuning models such as VGG19 through transfer learning. On the other hand, remote AD screening proposal eradicates the limitations of COVID-19 and facilitates secure patient assessment. They use key evaluation metrics like specificity, accuracy, and sensitivity to allow one to assess model performance and drive underlining clinical efficiency. Venugopalan et al. [8] research on the detection of AD by overcoming the limitations based on single-modal data and, in turn, advocate for the integration of multi-data that better improves the analysis of AD staging. The authors introduced a novel approach where MRI images, SNPs, and clinical test data were combined using DL techniques, including stacked denoising auto-encoders for clinical and genetic data and 3D-CNN for imaging. Cases were classified according to the three AD, MCI, and control groups, and a distinct kind of clustering and perturbation analysis pointed out the top features learned by deep models. Tested on ADNI data, this multi-modal approach outperformed standard models like random forests and SVMs, even bringing about distinctions in brain areas such as the hippocampus and the amygdala.

Ahila et al. [9] presented a study addressing the challenge imposed upon modern healthcare through AD. This they developed by creating an advanced CAD system built with CNNs trained on Positron Emission Tomography scans to enhance the system with diagnostic accuracy. Their model was trained on a set of 855 patient samples from the AD Neuroimaging Initiative (ADNI) database and tested for remarkable performance metrics with a sensitivity of 96%, specificity of 94%, and accuracy of 96%. Puente-Castro et al. [10] conceptualized early detection of AD and suggested a system that detects the existence of AD in MRI scans. They made use of transfer learning (TL) by using data from the ADNI dataset and OASIS dataset. Their model was trained to detect AD from sagittal MRIs with results that could be comparable to those gathered from horizontal-plane MRIs. This research shows the potential for early AD detection and monetary savings within DL models.

Zhang et al. [11] discussed detection regarding AD and MCI. They have proposed a novel DL approach that is CNN and a Two-stage Random RandAugment (TRRA) for data augmentation. It has included one method which generates heat maps using Grad-CAM++. This research provides solutions towards CAD methods for AD and MCI detection to problems like data leakage, overfitting, and an opaque diagnosis. Liu et al. [12] have offered a new ML method to detect the symptoms of AD. By incorporating several techniques of ML, they are working to make the diagnosis of AD very efficient as well as accurate for a better outcome in diagnosis. The research is a significant contribution to the field of medi-

cal diagnosis and serves to introduce potential improvements in AD diagnosis with potential far-reaching implications for both clinical practice and patient care. Chang et al., [13] analyzed various ML techniques along with biomarkers for AD diagnosis. In their review, they have particularly underlined the useful applicability of AI and ML tools to accurately diagnose AD. In addition to the classical biomarkers such as A β 42 and tau proteins, the paper references novel potential biomarkers implicated in various mechanisms that lead to AD pathology: neuronal injury, synaptic dysfunction, and neuroinflammation. The authors also mention that ML algorithms may be applicable to the area, pointing to a necessity for fast, inexpensive, and novel diagnostic tools.

Ebrahimighahnavieh et al. [14] developed a literature review on various DL techniques for AD detection. During the review, they highlighted the need for reliable and efficient diagnostic tools for the detection of AD. Following this review, the authors make a significant contribution to the DL techniques, unveiling the key features, methodologies, and the difficulties encountered while providing valuable perspectives for future studies in this area. Ji et al. [15] emphasized the need to detect AD earlier for proper intervention in slowing the disease progression. The authors applied DL algorithms for the task of pattern classification although the ML methods are highly dependent on manually extracted features and complex architectures. They proposed an ensemble model based on ConvNets. The authors demonstrated the DL techniques' potential within the domain of AD diagnosis. A sophisticated approach for the detection of AD using multi-modal ML was presented by Khan et al. [16]. Here, they proposed a five-stage ML pipeline that incorporates data transformation and feature selection along with a random forest classifier. The study contributed to understanding the possibility of automating diagnosis for clinical applications.

Orouskhani et al. [17] introduced a novel conditional deep triplet network for AD detection from structural MRI. They addressed this problem from having a few samples the dataset by using deep metric learning techniques. Their conditional loss function-based model, designed on top of VGG16, demonstrated superior performance compared to existing models. Saleh et al. [18] propose a class model for AD classification by using DenseNet with a healthcare decision support embedded into it. They use TL techniques to enhance their performance and demonstrate the generalization ability of the DenseNet model. Dua et al. [19] propounded a new integration method of LSTM-CNN-RNN in the detection of AD from MRI scans. They tried to classify the dementia levels efficiently as well as accurately for the early onset of medical intervention. This incorporates the utilization of CNNs in feature extraction and LSTM and RNN in sequence learning. They show the use of DL algorithms for enhancing the diagnosis of AD using ensemble techniques.

Saratxaga et al. [20] developed a DL-based method to predict AD from MRI images. They discussed how early diagnosis for timely intervention would be of extreme importance for AD. Their proposed method is a combined DL

and image processing technique that depicts some remarkable improvements in the diagnosis of AD. They achieved BAC of 0.93 in automated diagnosis and 0.88 for the classification of disease stages. Liu et al [21] proposed a novel approach that utilized depthwise separable CNNs (DSC) for the detection of AD from MRI scans. DSC reduces the complexity of the model and decreases the overhead of computations without compromising the performance. They could show that TL is feasible to be used on the ground with AlexNet and GoogLeNet in practice within mobile embedded systems.

The reviewed studies discussed various DL and ML approaches that have improved early detection and classification of AD by using biomedical imaging and multi-modal data. Transfer learning has been one of the most applied methods, using a pre-trained model: VGG19, DenseNet, GoogLeNet, etc, to leverage knowledge on sparse datasets. Features extraction in CNNs is also applied. Further reduction in the complexity of computations as compared to accuracy is achieved by depthwise separable CNNs. Ensemble models as a combination of CNNs, RNNs and LSTMs are also formed for sequential learning and multi-stage classification. Different kinds of data such as MRI scan data, SNPs, and clinical test data, provide multi-modal approaches improving the diagnostic power with capture of the various dimensions of the disease. Techniques like Grad-CAM++ and perturbation analysis have been used to apply interpretability to find important features in biomedical images. Techniques such as two-stage random RandAugment have been used for overcoming the problem of overfitting. Advanced architectures such as conditional deep triplet networks solved the problem of scarcity of data through metric learning. New pipelines that apply feature selection and transformation are being used for enhancing ML model performance. Collectively, these approaches advance the state of the art in terms of accuracy, scalability, and interpretability of AD detection systems toward effective clinical applications.

III. PROPOSED WORK

A. DATASET EXPLORATION

We used the OASIS project to facilitate neuroimaging datasets of the brain in this study. The research utilized cross-sectional MRI data for the young and middle-aged individuals, old age non-demented, and demented subjects through the OASIS-1 dataset. This dataset comprises MRI scans of 416 male and female subjects who are aged between 18 and 96. For every subject it covers 3 to 4 T1-weighted-scans acquired in a single session. It is also made up of scans of subjects who are assessed to be not demented and those diagnosed with mild to moderate AD.

It had been noticed that the OASIS dataset was majorly imbalanced in terms of classes as has been projected in Table 1. The MRI scans under various types of AD, such as 'MildDemented', 'ModerateDemented', 'NonDemented', 'VeryMildDemented', have been tabulated in Table 1 and graphically represented in Figure 3.

TABLE 1. Image Count of Each Type of Alzheimer's Disease MRI Scans Before Augmentation

Type of Alzheimer's Disease	Images Count
Non Demented	2560
Very Mild Demented	1792
Mild Demented	717
Moderate Demented	52

Balancing this is crucial for guaranteeing that DL models are learned properly. To that effect, the Augmented Alzheimer MRI Dataset [22] was used, which contains augmented images for every class of Alzheimer's MRI scans. Since augmentation balances the image distribution among all classes, it resolved the issue of class imbalance for this data set. The images' distribution for each type of AD has been presented in Table 2 and graphically represented in Figure 4.

TABLE 2. Image Count of Each Type of Alzheimer's Disease MRI Scans After Augmentation

Type of Alzheimer's Disease	Images Count
Non Demented	9600
Very Mild Demented	8960
Mild Demented	8960
Moderate Demented	6464

B. METHODOLOGY

We first preprocessed the augmented MRI images using four preprocessing methods, namely histogram equalization, median filtering, image resizing, and pixel normalization. Histogram equalization is employed to improve the contrast of the images. Median filtering reduces the noise within an image but does not blur the edges of an important structure. Resizing the dimension of all images passed to the model ensures that it receives images of equal dimensions. Normalization contributes to fast training of the model by eliminating unacceptably large ranges of input values, which might slow down learning. We then used the above-preprocessed images to train our proposed classifier model and classify the MRI images among one of the four AD types. We then evaluated the classification results using metrics like F1-score, recall, accuracy, and precision. The flow of work has been depicted in Figure 2.

C. PREPROCESSING

We preprocess the augmented images in the dataset by employing a pipeline that includes four stages: histogram equalization, median filtering, image resizing, and pixel normalization. The results following each preprocessing step of the Alzheimer's MRI image have been shown in Figure 5.

1) Histogram Equalization

Histogram Equalization is used for enhancing the contrast of an image. It redistributes pixel intensity levels. These are made to overcome difficulties of distinguishing among

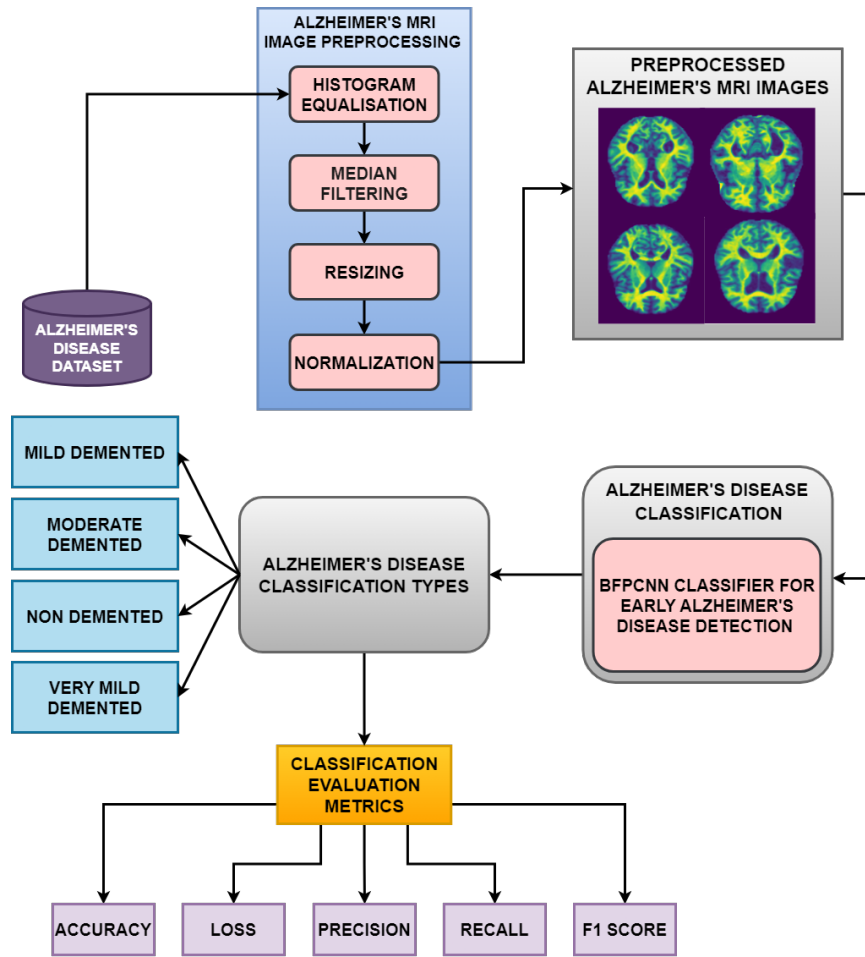


FIGURE 2. Overall Proposed System Workflow for Alzheimer's Disease Classification

Data Distribution of Alzheimer's Disease MRI Scans Before Augmentation

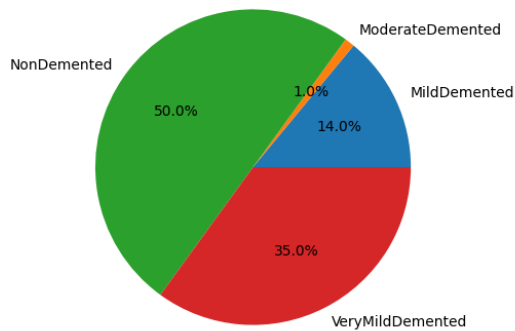


FIGURE 3. Graphical Representation of Data Distribution of Each Type of Alzheimer's Disease MRI Scans Before Augmentation

Data Distribution of Alzheimer's Disease MRI Scans After Augmentation

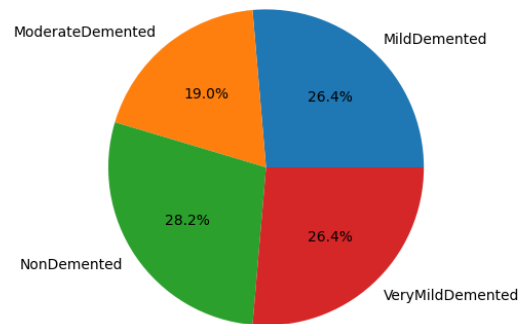


FIGURE 4. Graphical Representation of Data Distribution of Each Type of Alzheimer's Disease MRI Scans After Augmentation

several tissues or structures in MRI due to the wide range of intensity values arising in many of these MRI scans. Histogram equalization stretches the intensity values of the single

pixels across the possible range of intensity values.

$$\underbrace{I_{equalized}(x,y)}_{\text{Equalized Image}} = \underbrace{\left(\frac{L-1}{M \cdot N}\right)}_{\text{Scaling Factor}} \cdot \underbrace{\sum_{k=0}^{I_n(x,y)} \underbrace{H(k)}_{\text{Histogram}}}_{\text{Cumulative Distribution Function}} \quad (1)$$

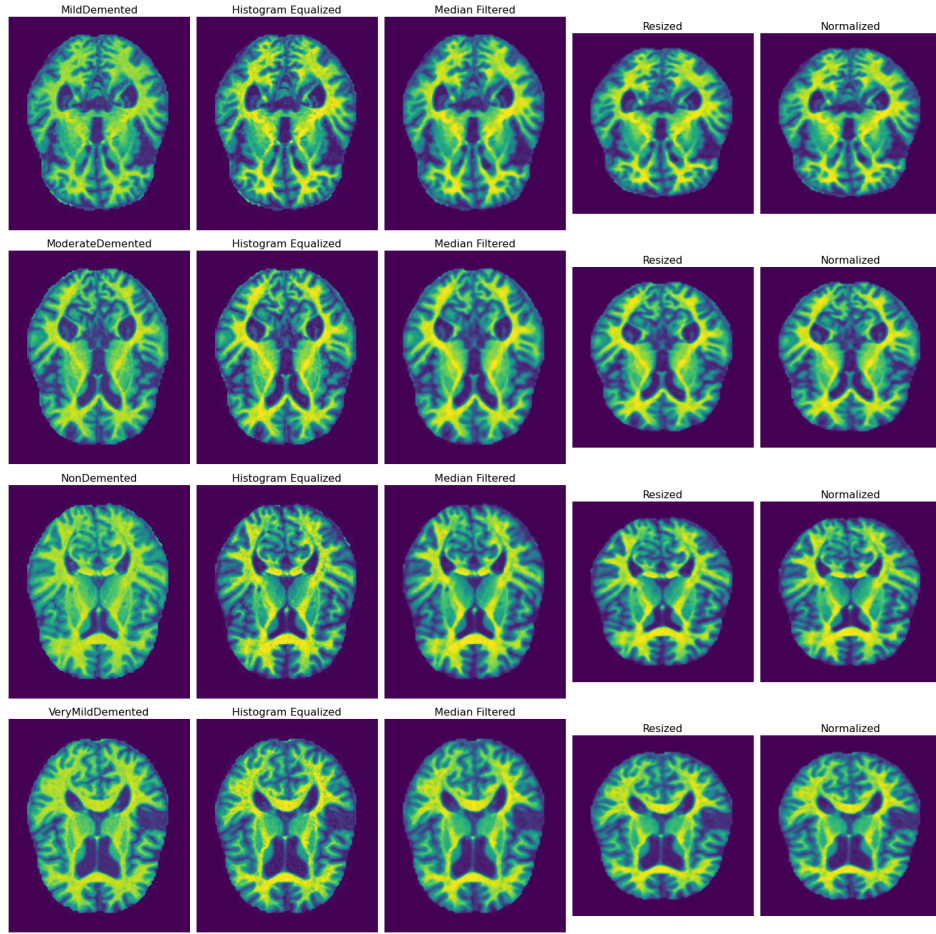


FIGURE 5. Alzheimer's Disease MRI Scans Observed After Each Pre-processing Step

This preprocessing technique ensures that the contrast between different tissues or structures in an MRI scan is enhanced with a view of identification and analysis. This helps where the original MRI scan has poor contrast, or some features are not distinguishing. The algorithmic workflow of this step is presented in Algorithm 1.

Algorithm 1: Histogram Equalization

Input: raw MRI image

Output: histogram equalized MRI image

Function histogramEqualization(image_{MRI}):

1. $hist_{image} \leftarrow \text{histogram of image}_{MRI}$
 2. Compute cumulative distribution from $hist_{image}$:

$$CDF(i) \leftarrow \sum_{j=0}^i P_r(j)$$
 3. Transform pixel intensity $I(x, y)$ at coordinate (x, y) using CDF :

$$I_{equalised}(x, y) \leftarrow \text{round} \left(\frac{CDF(I(x, y)) - CDF_{\min}}{CDF_{\max} - CDF_{\min}} \cdot (L - 1) \right)$$
 4. **For** each pixel p in image_{MRI} **do**
 Apply histogram equalization transformation on pixel p
 5. **End For**
 6. image_{heq} \leftarrow histogram equalized image
 7. **Return** image_{heq}
-

2) Median Filtering

AD MRI scans are susceptible to boundary effects and hence MRI scans tend to capture noise, such as Gaussian noise or salt-and-pepper noise, which degrades the image quality. Median filtering replaces every pixel by the median value of surrounding pixels, thereby preserving the edges and details of structures in the image and effectively removing noise-induced outliers. It will permit better general quality MRI scans for AD, which also means better extraction of features. The algorithmic workflow of median filtering is presented in Algorithm 2.

$$\underbrace{I_{out}(a, b)}_{\text{Output Image}} = \underbrace{\text{median}}_{\text{Median Operator}} \left(\underbrace{\{I_{in}(a + m, b + n) \mid m, n \in W\}}_{\text{Neighborhood Pixels}} \right) \quad (2)$$

Algorithm 2: Median Filtering

Input: histogram equalized MRI image
Output: median filtered MRI image
Function median_filter(image_{heq}):

1. $image \leftarrow image_{heq}$
2. $l \leftarrow$ length of image
3. $b \leftarrow$ breadth of image
4. $c \leftarrow$ channels of image
5. $w \leftarrow 3$ // window_size
6. $filtered_image \leftarrow$ create_empty_image(l, b)
7. $c_{img} \leftarrow$ image split into channel
8. **For** $i = 0$ to $l - 1$ **do**
 - For** $j = 0$ to $b - 1$ **do**
 - $c_{img} += image[i][j][1]$
- End For**
9. apply_median_filter(c_{img}, w)
10. **For** $i = 0$ to $l - 1$ **do**
 - For** $j = 0$ to $b - 1$ **do**
 - $image_{filtered} = [c_{img}[i][j]]$
- End For**
10. **End For**
11. **Return** $image_{filtered}$

End Function

3) MRI Image Resizing

Resizing is used to prevent overfitting in the model since the input data reduced its complexity. DL models must be a fixed size input; that is to say, all images presented to the model are the same size, which will be particularly important for batch processing, and it is consistent throughout the dataset. It also because resizing would take less time to train the model, providing better efficiency in model training. The algorithmic workflow of this preprocessing step is presented in Algorithm 3.

$$\underbrace{I_{out}(u, v)}_{\text{Resized Image}} = \underbrace{\sum_{i=0}^{M-1} \sum_{j=0}^{N-1} \underbrace{I_{in}(i, j)}_{\text{Input Image}} \cdot \underbrace{K(u - S_u(i), v - S_v(j))}_{\text{Interpolation Kernel}}}_{\text{Interpolation Sum}}
 \quad (3)$$

4) Pixel Normalization

Pixel Normalization normalizes pixel values in the images between the range (0, 1). It reduces large ranges of input values that can impair learning and brings the model to convergence faster in training. After normalizing input images, gradients tend to be more stable and less prone to getting vanishing effects in the gradient descent optimization algorithms applied in DL models. This also prevents overfitting since it makes sure that the model learns the patterns of the data and does not memorize the pixel values. The algorithmic workflow of

Algorithm 3: Image Resizing

Input: median filtered MRI image
Output: resized MRI image
Function resize(image_{filtered}):

1. $h \leftarrow$ height of image_{filtered}
2. $w \leftarrow$ width of image_{filtered}
3. $t \leftarrow$ target size
4. Calculate scaling factor:
 - $S_H \leftarrow \frac{t}{h}$
 - $S_W \leftarrow \frac{t}{w}$
5. **For each** pixel at coordinates (x, y) **do**
 - $i' \leftarrow \lfloor x \cdot S_H \rfloor$
 - $j' \leftarrow \lfloor y \cdot S_W \rfloor$
 - $image_{resized}(i', j') \leftarrow image_{MRI}(i, j)$
6. **End For**
7. **Return** $image_{resized}$

End Function

pixel normalization is presented in Algorithm 4.

$$\underbrace{I_{norm}(i, j)}_{\text{Normalized Pixel}} = \frac{\underbrace{I(i, j)}_{\text{Pixel Value}}}{\underbrace{255.0}_{\text{Maximum Pixel Value}}} \quad (4)$$

Algorithm 4: Normalization

Input: resized MRI image
Output: normalized MRI image
Function normalize_image(image_{resized}):

1. $l \leftarrow$ length of image_{resized}
2. $b \leftarrow$ breadth of image_{resized}
3. $c \leftarrow$ channels of image_{resized}
4. $normalisation_value \leftarrow 255$
5. $normalised_image \leftarrow$ create_empty_image(l, b)
6. **For** $i = 0$ to $l - 1$ **do**
 - For** $j = 0$ to $b - 1$ **do**
 - For** $k = 0$ to $c - 1$ **do**
 - $normalised_image[i][j][k] \leftarrow \frac{image_{resized}[i][j][k]}{255}$
 - End For**
- End For**
7. **Return** $normalised_image$

End Function

D. GRANULAR FEATURE INTEGRATION

Detecting Alzheimer's Disease (AD) through MRI scans demands models capable of extracting hierarchical features $\mathcal{F} = \{f_1, f_2, \dots, f_n\}$ that span both macro- and micro-level brain structures. Conventional Convolutional Neural Networks (CNNs), formulated as $f_\theta(x) = \sigma(W * x + b)$ with convolutional weights W and biases b , often excel at low-level feature extraction but struggle with high-level granular details critical for AD detection. To overcome this, we propose Granular Feature Integration (GFI), a mechanism that fuses residual learning $R(x) = x + \mathcal{H}(x)$ with multi-scale processing $M(x) = \bigoplus_{s \in S} \psi_s(x)$, where S denotes the set

of scales and ψ_s represents convolutional transformations at scale s .

Formally, GFI can be represented as a composite function:

$$GFI(x) = R(I(x)), \quad (5)$$

where $R(x) = x + F(x, W)$ denotes the residual mapping and $I(x) = \bigoplus_{k=1}^n \delta_k(x)$ aggregates multi-scale features through convolutions δ_k with kernel sizes $k \in \{1, 3, 5, 7\}$. The residual pathways ensure that the gradient $\nabla_x L$ remains bounded, thus solving the vanishing gradient problem for deep architectures, while the inception modules allow the network to process spatial hierarchies by varying the receptive field r_k .

By integrating these two mechanisms, the model captures a more expressive feature space:

$$\mathcal{F}_{\text{granular}} = \{f_{\text{global}}, f_{\text{local}}\}, \quad (6)$$

where f_{global} represents macroscopic brain structures, and f_{local} encodes subtle neurodegenerative markers.

E. PROPOSED BI-FOCAL PERSPECTIVE CONVOLUTIONAL NEURAL NETWORK (BFPCNN)

In this section, we present our proposed Bi-Focal Perspective CNN for Early Alzheimer's Detection. We feed the pre-processed MRI images to our proposed model, and then our model is going to output the respective predicted probabilities for each disease type. The overall architecture of the proposed BFPCNN is shown in Figure 6.

To get attention to detail in MRI scans along with eliminating vanishing gradients along layers, our model has focused on a Bi-Focal Perspective mechanism. For efficiently extracting fine details and raising feature representation, we have incorporated Granular Feature Integration to improve the overall capability of the model to capture features of different scales. It has the ability to correctly lift out the desired features and classify very well among the varieties of AD, thus improving the performance significantly. Our model begins with an initial convolutional block, consisting of a convolution layer that utilizes 64 filters and a kernel of size 7x7, followed by a max-pooling layer. The basic features the model identifies include the layout of the brain and contours of various brain regions from the MRI image. Then comes the next convolutional block, which consists of a Batch Normalization layer and further convolutional layers with heterogeneous parameters. This block helps the model to refine the initial features and in the identification of gray and white matter, which is basic for recognizing anatomical features in the brain.

$$\underbrace{\text{Conv}(I_{(i,j)}, F)}_{\text{Convolution Operation}} = \sum_{m=0}^{M-1} \sum_{n=0}^{N-1} \underbrace{I_{(i+m,j+n)}}_{\text{Input feature map}} \cdot \underbrace{F_{(m,n)}}_{\text{Filter}} + \underbrace{b}_{\text{Bias}} \quad (7)$$

$$\underbrace{\text{MaxPooling}(O)_{(i,j)}}_{\text{Max Pool Operation}} = \max_{p=0}^{k-1} \max_{q=0}^{k-1} \underbrace{I_{(i-s+p,j-s+q)}}_{\text{Input feature map}} \quad (8)$$

$$\underbrace{\text{BN}(x)}_{\text{Batch Normalization}} = \underbrace{\gamma}_{\text{Adaptable parameter}} \left(\frac{\underbrace{x}_{\text{Input}} - \underbrace{\mu}_{\text{Mean}}}{\sqrt{\underbrace{\sigma^2}_{\text{Variance}} + \underbrace{\epsilon}_{\text{constant}}}} \right) + \underbrace{\beta}_{\text{Adaptable parameter}} \quad (9)$$

The feature map is then passed to an inception block [23]. This allows expansion in the capacity of capturing various features at different scales. It consists of parallel paths to convolutional layers with varying kernel sizes (5x5, 1x1, and 3x3) and max pooling layers. This helps the model extract fine details while also focusing on broader contextual information simultaneously. Smaller-sized kernels look at the local features and try to monitor slight changes in the hippocampal region of the brain. Larger-size kernels look at the ventricles enlargement overall, which is believed to be a typical sign in later stages of Alzheimer's. These parallel paths then get concatenated to form one feature vector that comes from the inception block. The algorithmic workflow of inception block is presented in Algorithm 5.

$$\underbrace{\text{concat}(X, Y)}_{\text{concatenation operation}} = \begin{cases} \underbrace{X_{(p,q,r)}}_{\text{input feature map from X}} & \text{if } 1 \leq r \leq \text{depth}(X), \\ \underbrace{Y_{(p,q,r-\text{depth}(X))}}_{\text{input feature map from Y}} & \text{if } \text{depth}(X) < r \leq \text{depth}(X) + \text{depth}(Y). \end{cases} \quad (10)$$

Algorithm 5: Inception Block

Function inceptionBlock(input):

1. $x_{11} \leftarrow$ number of filters for path 1 conv₁
2. $x_{21} \leftarrow$ number of filters for path 2 conv₁
3. $x_{22} \leftarrow$ number of filters for path 2 conv₂
4. $x_{31} \leftarrow$ number of filters for path 3 conv₁
5. $x_{32} \leftarrow$ number of filters for path 3 conv₂
6. $x_{41} \leftarrow$ number of filters for path 4 conv₁
7. $y \leftarrow \text{kernel size}$
8. $z \leftarrow \text{convolution stride}$
9. $p_1 \leftarrow \text{conv2D}(x_{11}, y, z)(\text{input})$
10. $p_2 \leftarrow \text{conv2D}(x_{21}, y, z)(\text{input})$
11. $p_2 \leftarrow \text{conv2D}(x_{22}, y, z)(p_2)$
12. $p_3 \leftarrow \text{conv2D}(x_{31}, y, z)(\text{input})$
13. $p_3 \leftarrow \text{conv2D}(x_{32}, y, z)(p_3)$
14. $p_4 \leftarrow \text{maxPooling}(2, 2)(\text{input})$
15. $p_4 \leftarrow \text{conv2D}(x_{41}, y, z)(p_4)$
16. $\text{output} \leftarrow \text{concatenate}(p_1, p_2, p_3, p_4)(\text{input})$
17. **Return** output

End Function

Following this initialization block, there is a self-attention mechanism [24] to determine the importance of features relative to one another. The models are, therefore, enabled to focus in these areas that often reflect typical features of AD like altered brain volume. The algorithmic workflow of self-attention is presented in Algorithm 6.

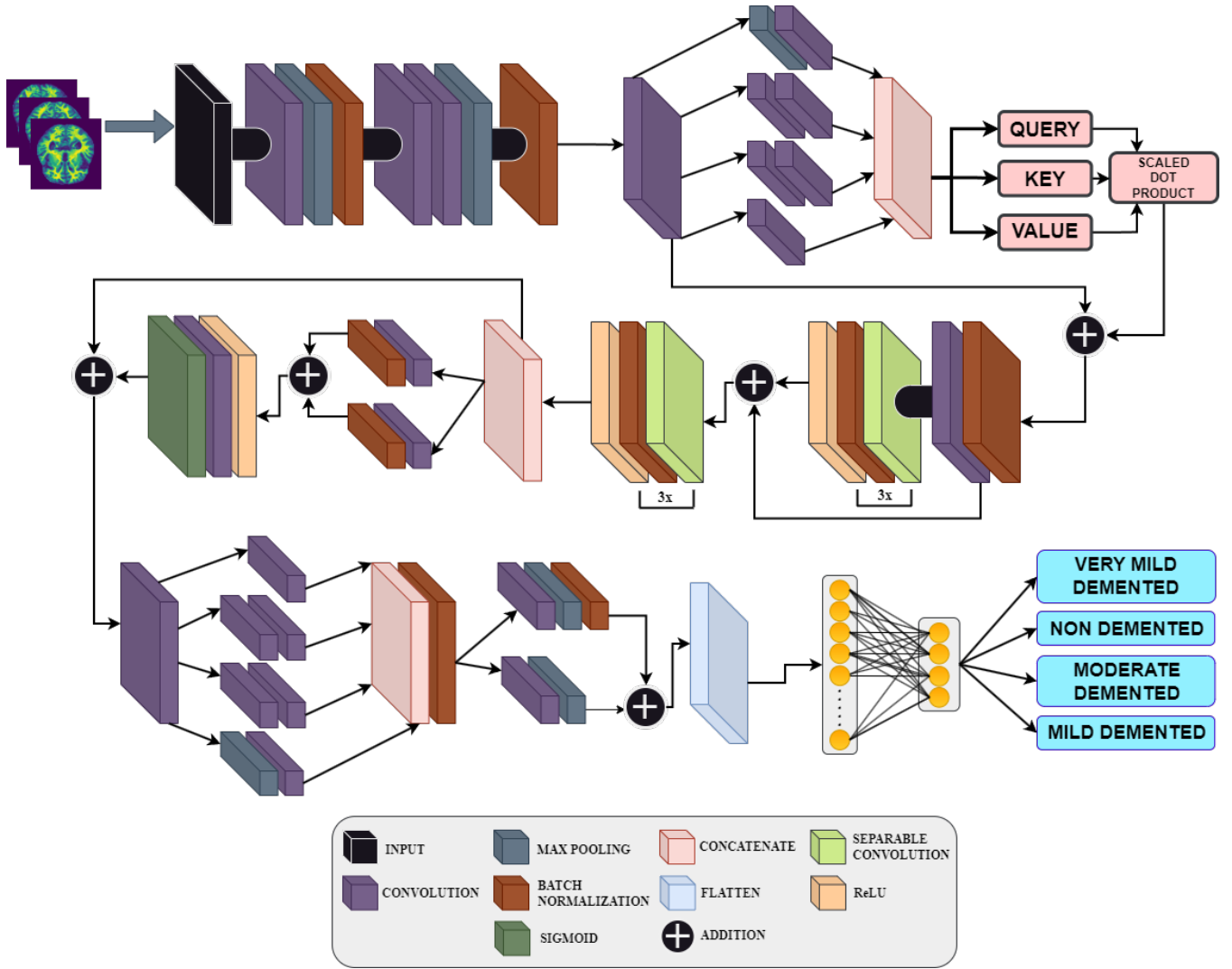


FIGURE 6. Proposed BFPCNN Layer Architecture for AD Classification

$$\underbrace{\alpha_{ij}}_{\text{Attention weight for position } (i,j)} = \underbrace{\text{softmax} \left(\frac{\underbrace{K^T Q}_{\text{Dot product of key and query}}}{\underbrace{d_k}_{\text{Dimensionality of key vectors}}} \right)}_{\text{Softmax normalization}} \underbrace{V}_{\text{Value matrix}} \quad (11)$$

This feature map then passes through separable convolutional blocks with multiple residual connections [25] ensuring proper gradients flow through the neural network. Separable convolutional layers split the convolutions into depthwise and pointwise parts, which ensure minimal computational complexity while retaining the capability to capture intricate spatial dependencies from the MRI scan. Batch normalization normalizes the activations of the layer, ensuring that the learning is stabilized and the internal covariate shifts are reduced. ReLU activation functions induce a nonlinearity in the models. This is necessary for extracting more complex

Algorithm 6: Self Attention

Function selfAttention(input):

1. $q \leftarrow$ query vector
2. $k \leftarrow$ key vector
3. $v \leftarrow$ value vector
4. $s \leftarrow$ scaling parameter
5. $a \leftarrow (q @ k.transpose(-2, -1)) * s$
6. $matrix_{qk} \leftarrow \text{softmax}(a)$
7. $z \leftarrow \text{Dropout}(a)$
8. $z \leftarrow \text{fullyConnected}(z)$
9. $z \leftarrow \text{Dropout}(z)$
10. **Return** $z.matrix_{qk}$

End Function

relationships from the features extracted.

$$\underbrace{\text{ReLU}(x)}_{\text{Rectified Linear Unit Activation}} = \begin{cases} \underbrace{x}_{\text{Feature map}} & \text{if } x > 0 \\ 0 & \text{otherwise} \end{cases} \quad (12)$$

After the separable convolutional blocks, a spatial attention mechanism [26] is applied. It emphasizes the crucial regions of interest in the spatial domain of the feature map. These uses of both spatial attention as well as self-attention, coming under the Bi-Focal Perspective, help the model pay attention to local and global features. As spatial attention pays attention to the spatial domain, self-attention does its work in enabling the model to analyze the association between features across the full feature map and capture subtle changes for analysis. The algorithmic workflow of spatial-attention is presented in Algorithm 3. The combined application of both mechanisms helps the Bi-Focal Perspective aid the model in understanding the subtle details as well as developing an understanding of the bigger picture in the MRI scan.

Algorithm 7: Spatial Attention

Function spatialAttention(input):

1. $d \leftarrow$ dilation convolution count

2. $x \leftarrow$ number of filters for conv

3. $y \leftarrow$ kernel size

4. $z \leftarrow$ convolution stride

5. **For** $i = 1$ to d **do**

$t_i \leftarrow \text{conv}(f, k, s)(\text{input})$

$t_i \leftarrow \text{batchNorm}(t_i)$

6. **End For**

7. $\text{output} \leftarrow \sum_i t_i \quad \forall t \in [1, 2, \dots, d]$

8. **Return** output

End Function

This is further followed by a second inception block that complements the spatial attention mechanism by providing an overall view of the MRI data at different levels. Then for even better learning of residual functions, a residual block has been implemented. Then there exists a flattening layer used for flattening down the output to a dimension for dense processing in a dense layer. Finally, a softmax activation function returns a probability distribution of the input MRI image over the different classes – 'Mild Demented', 'Moderate Demented', 'Non-Demented', and 'Very Mild Demented'.

$$\underbrace{S(I_i)}_{\text{Softmax Output}} = \frac{\underbrace{e^{I_i}}_{\text{Exponentiated Input}}}{\underbrace{\sum_{j=1}^N e^{I_j}}_{\text{Sum of Exponentiated Inputs}}} \quad (13)$$

The parameter specifications of the proposed BFPCNN are presented in Table 3.

TABLE 3. Proposed Model Parameter Specifications

Parameters	Coefficients
Total number of layers	68
Learning rate	0.001
Epochs	100
Batch size	128
Total Parameters	153,066,236

IV. RESULTS AND DISCUSSION

A. EXPERIMENTAL SETUP

In this section, we discuss the performance of the proposed model by comparing it with other models in the same domain. We carried out our experiments on a system characterized by the following specifications: Operating System - Linux 5.15.133; CPU - AMD EPYC 7763 with 128 CPU(s) and x86_64 architecture; GPU - AMD Radeon Instinct Model 1; with 64 Core(s) per socket, 2 Socket(s), and 1 Thread(s) per core. This information is summarized in Table 4.

TABLE 4. Configuration and Specifications of the System Used

Component	Specification
Operating System	Linux 5.15.133
CPU	AMD EPYC 7763
Architecture	x86_64
CPU(s)	128
GPU	AMD Radeon Instinct
Model	1
Core(s) per socket	64
Socket(s)	2
Thread(s) per core	1

B. EVALUATION METRICS

Our proposed model's performance for detecting AD was evaluated using the following metrics.

1) Accuracy

Accuracy can be defined as the evaluation metric which is responsible for determining how close the predicted value is to its true value. It is computed as a ratio between the count of true positives to the count of all the samples given to the model.

$$\underbrace{\text{Accuracy}}_{\text{Accuracy}} = \frac{\underbrace{\sum_{i=1}^N \underbrace{TP_i}_{\text{TruePositives}} + \underbrace{TN_i}_{\text{TrueNegatives}}}_{\text{CorrectPredictions}}}{\underbrace{N}_{\text{TotalSamples}}} \quad (14)$$

Where n represents the number of classes present in the dataset, TP represents the number of true positive samples, and FP, FN, and TN represent the number of false positive, false negative and true negative samples respectively.

2) Precision

To measure the model's performance which involves the identification ability of only the relevant instances, the precision

metric is taken into account and is considered critical when there is an increase in the number of false positives. It denotes the ratio of true positives to the sum of true positives and false positives.

$$\underbrace{\text{Recall}}_{\text{Recall for Class } c} = \frac{\overbrace{TP_c}^{\text{True Positives for Class } c}}{\underbrace{TP_c}_{\text{True Positives for Class } c} + \underbrace{FN_c}_{\text{False Negatives for Class } c}} \quad (15)$$

3) Recall

To measure the model's performance which involves the capture ability of all the relevant instances, the recall metric is taken into account and is considered critical when there is an increase in the number of false negatives. It represents the proportion of true positives relative to the sum of true positives and false negatives.

$$\underbrace{\text{Precision}}_{\text{Precision for Class } c} = \frac{\overbrace{TP_c}^{\text{True Positives for Class } c}}{\underbrace{TP_c}_{\text{True Positives for Class } c} + \underbrace{FP_c}_{\text{False Positives for Class } c}} \quad (16)$$

4) F1-Score

The F1-Score integrates precision and recall into a unified metric, providing a balanced assessment of the model's performance. It is calculated as the harmonic mean of precision and recall.

$$\underbrace{\text{F1 Score}}_{\text{F1 Score for Class } c} = 2 \cdot \frac{\text{recall} \cdot \text{precision}}{\text{recall} + \text{precision}} \quad (17)$$

Our classifier was trained for 100 epochs, and the performance metrics obtained at every epoch are recorded and plotted against each epoch to observe the variation in the model performance compared to its previous iterations. The scores obtained for accuracy, precision, recall and F1-score are illustrated in Figures 7, 8, 9, and 10 respectively. The categorical cross entropy loss function was utilized to determine the loss incurred during training, and the obtained loss at each epoch is illustrated in Figure 11.

The above graphs show that our proposed model has demonstrated robust and exceptional performance during its learning phase. The model learns most of the features effectively up to around 30 epochs, after which it starts to converge. The proposed model achieved a precision of 99.3%, a recall of 99.6%, an F1-score of 99.3%, and an accuracy of 99.2%. These metrics indicate that the proposed model has learned the data well while being able to apply it to unseen scenarios effectively as seen from the validation curve. The Bi-Focal Perspective and Granular Feature Integration mechanisms integrated into the model allow it to effectively extract spatial dependencies from the MRI images, while also being able to apply more focus to specific parts of the image by comparing various aspects of the same image and ensuring proper flow of gradients along the network.

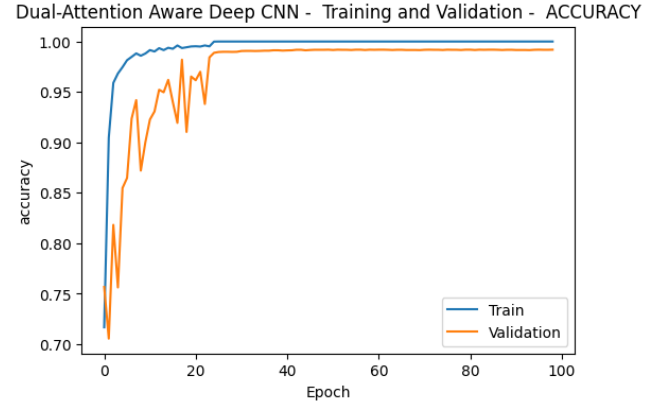


FIGURE 7. Training and validation accuracy plots for the Proposed Model

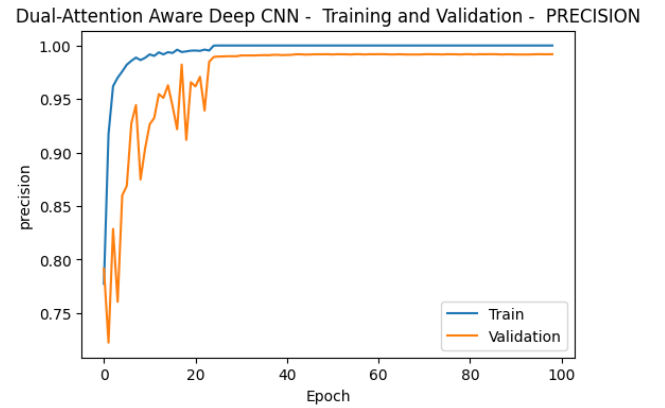


FIGURE 8. Training and validation precision plots for the Proposed Model

C. DISCUSSIONS

The confusion matrix for the testing data using our trained proposed model is shown in Figure 10. This type of matrix displays values as proportions or percentages, making it easy to compare classification performance across different classes. With values ranging from 0 to 1, it simplifies interpretation. The matrix illustrates the classifier's performance for the four AD classes: "Mild Demented," "Moderate Demented," "Non-Demented," and "Very Mild Demented." Each column represents the predicted class, while each row represents the actual (True) class. The main diagonal values indicate the percentage of correctly classified cases, whereas the off-diagonal values represent misclassified cases.

It can be observed from the confusion matrix, illustrated in Figure 10, that our model has impressive accuracy across all classes. The majority of samples were correctly classified as shown by values close to one along the diagonal. For instance, for "Mild Demented" class, the model yielded a 0.99 true positive rate (TPR), implying that 99% of samples were correctly classified. Again, for "Moderate Demented" class, had a TPR of 0.98 showing that 98% of cases were correctly classified. The 'Non-Demented' class also had a high TPR of 0.98 expressing correct classification at 98%.

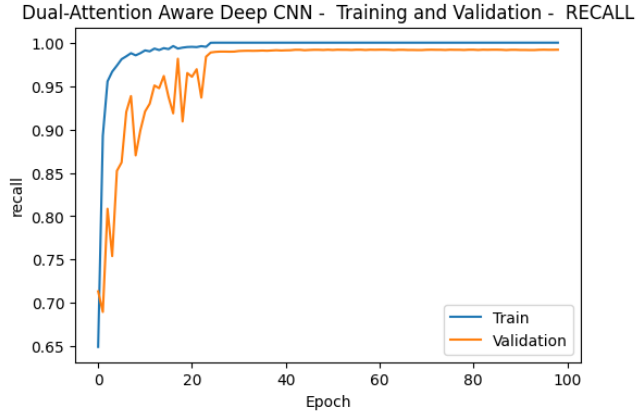


FIGURE 9. Training and validation recall plots for the Proposed Model

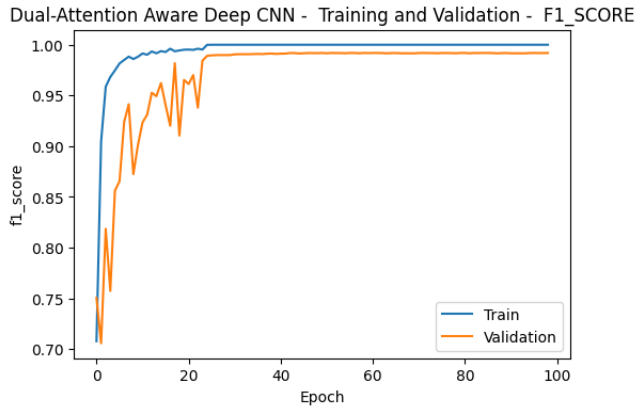


FIGURE 10. Training and validation F1-score plots for the Proposed Model

Lastly, the “Very Mild Demented” class had a 0.99 TPR, indicating that there was an accurate identification of about 99% of samples in this category. In conclusion, these levels of misclassification rates indicated how effective these models are in differentiating various stages of Alzheimer’s ailment because they have small values off-diagonal.

Our proposed model was evaluated against other SOTA CNNs - DenseNet121 [27], EfficientNetV2 [28], InceptionV3 [23], InceptionResNetV2 [29], MobileNetV2 [30], MobileNet [31], NASNetMobile [32], ResNet50 [25], VGG16 [33], and Xception [34]. The comparison aimed to assess our model against established CNN benchmarks used as baselines for AD detection. The models were trained using the augmented OASIS dataset, and the results have been tabulated in Table 5. Evaluation of these models was based on key metrics such as Precision (Prec), Accuracy (Acc), F1-score (F1), and Recall (Rec).

From Table 5, we can infer that our proposed model has performed significantly well compared to other baseline CNN-based models. DenseNet121 benefits from dense connectivity, which aids in feature reusing; however, it impacts its ability to accurately identify particular Alzheimer’s features such as amyloid plaques and neurofibrillary tangles.

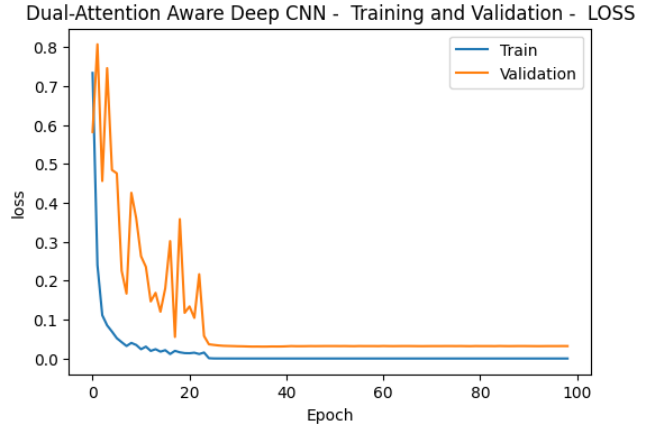


FIGURE 11. Training and validation loss plots for the Proposed Model

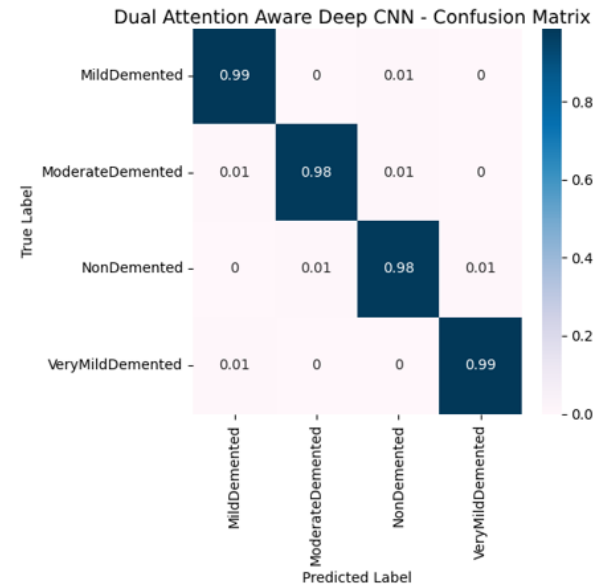


FIGURE 12. Confusion Matrix Obtained from the Proposed Model

EfficientNetV2 tends to overfit, due to challenges in capturing the subtle features of AD, such as the minor changes in brain structure or variations in brain activity observed in MRI scans. InceptionV3 is designed for efficient computation, making it incapable of analyzing the multidimensional characteristics of Alzheimer’s MRI data, especially in detecting subtle neural network disruptions or changes in brain volume. Despite its complicated structure, there is an inadequate match between InceptionResNetV2 and the demand to distinguish precise disease-specific features such as synaptic loss or alterations in brain function.

The lightweight design of MobileNetV2 is not as good at detailed analysis to identify conditions like the early symptoms of AD, that is, mild cognitive impairment (MCI) or minor hippocampal atrophy. By focusing on efficiency, MobileNet sacrifices the depth needed for thorough feature ex-

TABLE 5. Proposed model performance comparison against pretrained CNNs during Training and Validation Phase

Model	Training Phase Metrics				Validation Phase Metrics			
	Accuracy	Precision	Recall	F1	Accuracy	Precision	Recall	F1
DenseNet121	0.9912	0.9913	0.9921	0.9914	0.9513	0.9622	0.9614	0.9625
EfficientNetV2	0.9901	0.9912	0.9922	0.9913	0.9312	0.9423	0.9312	0.9311
InceptionV3	0.9921	0.9911	0.9923	0.9912	0.9611	0.9613	0.9712	0.9613
InceptionResNetV2	0.9512	0.9513	0.9623	0.9612	0.9323	0.9424	0.9313	0.9312
MobileNetV2	0.9811	0.9822	0.9812	0.9823	0.8913	0.9014	0.9114	0.9013
MobileNet	0.9712	0.9813	0.9723	0.9814	0.8914	0.9015	0.9013	0.9014
NASNetMobile	0.9922	0.9923	0.9913	0.9924	0.8915	0.8814	0.8823	0.8824
ResNet50	0.9912	0.9813	0.9813	0.9814	0.9213	0.9114	0.9114	0.9113
VGG16	0.8813	0.8914	0.8814	0.8813	0.7814	0.7915	0.7814	0.7813
Xception	0.9913	0.9914	0.9924	0.9913	0.9614	0.9523	0.9614	0.9613
Proposed CNN	0.9923	0.9914	0.9914	0.9924	0.9913	0.9923	0.9953	0.9933

traction from Alzheimer's MRI images. The NASNetMobile, designed for mobile applications, is not fine-tuned enough to capture all the significant intersections that would signal Alzheimer's such as altered white matter integrity or cortical atrophy. ResNet50's depth and focus may make it difficult to learn about such things as hippocampal atrophy. Simplicity and the relative shallowness of VGG16 struggle with such detailed analysis where ventricular enlargement is observed resulting in low validation accuracy tests. Xception does not fully exploit the spatial relationships that are key to identifying specific indicators of Alzheimer's, like brain atrophy patterns or connectivity between brain regions. Our proposed model stands out given that it combines dual spatial and self-attention mechanisms, providing a unique ability to identify amyloid deposition, neural network disruptions, and hippocampal atrophy among other critical features. These improvements assist in capturing intricate and heterogeneous pathology patterns typical for AD as seen from MRI scans.

Our model was also compared with existing research in the area of AD detection using ML and DL. The comparison of performance between these models is detailed in Table 6.

TABLE 6. Proposed model performance metrics comparison with existing research

Model	Accuracy (%)	Recall (%)	F1 (%)	Precision (%)
CNN, RNN, LSTM Ensemble [19]	89.75	91.07	89.08	89.16
CNN, RNN, LSTM Bagged Ensemble [19]	92.22	92.57	91.87	91.92
Wavelet Entropy, MLP and BBO [35]	92.41	92.47	92.30	92.14
DEMNET without SMOTE [36]	85.43	88.32	83.32	80.11
DEMNET with SMOTE [36]	95.23	95.21	95.27	96.43
Proposed Method	99.12	99.54	99.31	99.21

From Table 6, we can infer that the CNN, RNN, and

LSTM Ensemble model attained an accuracy of 89.75%, with recall, precision, and F1 scores of 91.07%, 89.16%, and 89.08%, respectively. The CNN, RNN, and LSTM Bagged Ensemble showed a slight improvement, with precision of 91.92%, accuracy of 92.22%, F1 score of 91.87%, and recall of 92.57%. The Wavelet Entropy, Multilayer Perceptron, and Biogeography-Based Optimization model performed comparably, achieving an accuracy of 92.4%, precision of 92.14%, recall of 92.47%, and an F1 score of 92.3%. DEMNET without SMOTE had the lowest performance among the compared models, with a recall of 88.32%, precision of 80.11%, an F1 score of 83.32%, and an accuracy of 85.43%. However, when SMOTE was applied to DEMNET, the model's performance significantly improved, achieving a recall of 95.21%, precision of 96.43%, an F1 score of 95.27%, and an accuracy of 95.23%. Our proposed methodology demonstrates notable performance, with a recall of 99.54%, precision of 99.21%, F1 score of 99.31%, and an accuracy of 99.12%. This is because the model offers advanced feature extraction capabilities, and that this would help in identifying indicative images which would have features of hippocampal atrophy and cortical thinning. These enable the model to find very subtle and complex patterns and information associated with AD much more effectively.

V. CONCLUSION AND FUTURE SCOPE

AD is one among the slowly progressing and irreversible neurodegenerative disorders leading to serious complications like cell death in the neuronal structure. We hereby present a novel classification method for the diagnosis of AD using the application of Bi-Focal Perspectives and Granular Feature Integration as a promising approach toward early detection and a better diagnostics method. The high accuracy and precision scores of our proposed model indicate robustness and relia-

bility in identifying and classifying AD. Graph Neural Networks, Graph Attention Networks, can therefore be explored for further improvement to the model's performance in future works. Capabilities of GATs and GNNs will help us capture the more complex relationships and dependencies within the neuroimaging data by utilizing both inter-regional and intra-regional connections. In addition, the models will be refined with more extensive and diverse datasets. Improved accuracy and generalization will be achieved as a result, promising better application in not only improving the diagnosis of Alzheimer's but also neurodegenerative disease research as a whole.

REFERENCES

- [1] H.-I. Suk, S.-W. Lee, and D. Shen, "Hierarchical feature representation and multimodal fusion with deep learning for ad/mci diagnosis," *NeuroImage*, vol. 101, pp. 569–582, 2014.
- [2] T. Jo, K. Nho, S. L. Risacher, and A. J. Saykin, "Deep learning detection of informative features in tau pet for alzheimer's disease classification," *BMC Bioinformatics*, vol. 21, no. S21, 2020.
- [3] S. Liu, S. Liu, W. Cai, S. Pujol, R. Kikinis, and D. Feng, "Early diagnosis of alzheimer's disease with deep learning," in *2014 IEEE 11th International Symposium on Biomedical Imaging (ISBI)*. IEEE, 2014, pp. 1015–1018.
- [4] S. Spasov, L. Passamonti, A. Duggento, P. Liø, and N. Toschi, "A parameter-efficient deep learning approach to predict conversion from mild cognitive impairment to alzheimer's disease," *NeuroImage*, 2019.
- [5] T. Jo, K. Nho, and A. J. Saykin, "Deep learning in alzheimer's disease: Diagnostic classification and prognostic prediction using neuroimaging data," *Frontiers in Aging Neuroscience*, vol. 11, 2019.
- [6] D. S. Marcus, T. H. Wang, J. Parker, J. G. Csernansky, J. C. Morris, and R. L. Buckner, "Open access series of imaging studies (oasis): Cross-sectional mri data in young, middle aged, nondemented, and demented older adults," *Journal of Cognitive Neuroscience*, vol. 19, no. 9, pp. 1498–1507, sep 2007. [Online]. Available: <http://dx.doi.org/10.1162/jocn.2007.19.9.1498>
- [7] H. A. Helaly, M. Badawy, and A. Y. Haikal, "Deep learning approach for early detection of alzheimer's disease," *Cognitive Computation*, vol. 14, no. 5, pp. 1711–1727, nov 2021. [Online]. Available: <http://dx.doi.org/10.1007/s12559-021-09946-2>
- [8] J. Venugopalan, L. Tong, H. R. Hassanzadeh, and M. D. Wang, "Multimodal deep learning models for early detection of alzheimer's disease stage," *Scientific Reports*, vol. 11, no. 1, feb 2021. [Online]. Available: <http://dx.doi.org/10.1038/s41598-020-74399-w>
- [9] A. A. P. M. M. Hamdi, S. Bourouis, R. Kulhanek, and F. Mohamed, "Evaluation of neuro imaging for the diagnosis of alzheimer's disease using deep learning neural network," *Frontiers in Public Health*, vol. 10, feb 2022. [Online]. Available: <http://dx.doi.org/10.3389/fpubh.2022.834032>
- [10] A. Puente-Castro, E. Fernandez-Blanco, A. Pazos, and C. R. Munteanu, "Automatic assessment of alzheimer's disease diagnosis based on deep learning techniques," *Computers in Biology and Medicine*, vol. 120, p. 103764, may 2020. [Online]. Available: <http://dx.doi.org/10.1016/j.combiomed.2020.103764>
- [11] F. Zhang, B. Pan, P. Shao, P. Liu, S. Shen, P. Yao, and R. X. Xu, "A single model deep learning approach for alzheimer's disease diagnosis," *Neuroscience*, vol. 491, pp. 200–214, 2022. [Online]. Available: <https://www.sciencedirect.com/science/article/pii/S030645222200149X>
- [12] L. Liu, S. Zhao, H. Chen, and A. Wang, "A new machine learning method for identifying alzheimer's disease," *Simulation Modelling Practice and Theory*, vol. 99, p. 102023, feb 2020. [Online]. Available: <http://dx.doi.org/10.1016/j.simpat.2019.102023>
- [13] C.-H. Chang, C.-H. Lin, and H.-Y. Lane, "Machine learning and novel biomarkers for the diagnosis of alzheimer's disease," *International Journal of Molecular Sciences*, vol. 22, no. 5, p. 2761, mar 2021. [Online]. Available: <http://dx.doi.org/10.3390/ijms22052761>
- [14] M. A. Ebrahimighahnavieh, S. Luo, and R. Chiong, "Deep learning to detect alzheimer's disease from neuroimaging: A systematic literature review," *Computer Methods and Programs in Biomedicine*, vol. 187, p. 105242, apr 2020. [Online]. Available: <http://dx.doi.org/10.1016/j.cmpb.2019.105242>
- [15] H. Ji, Z. Liu, W. Q. Yan, and R. Klette, "Early diagnosis of alzheimer's disease using deep learning," in *Proceedings of the 2nd International Conference on Control and Computer Vision (ICCCV 2019)*. ACM, jun 2019. [Online]. Available: <http://dx.doi.org/10.1145/3341016.3341024>
- [16] A. Khan and S. Zubair, "An improved multi-modal based machine learning approach for the prognosis of alzheimer's disease," *Journal of King Saud University – Computer and Information Sciences*, 2020.
- [17] M. Orouskhani, C. Zhu, S. Rostamian, F. Shomal Zadeh, M. Shafiei, and Y. Orouskhani, "Alzheimer's disease detection from structural mri using conditional deep triplet network," *Neuroscience Informatics*, 2020.
- [18] A. W. Saleh and G. Gupta, "An alzheimer's disease classification model using transfer learning densenet with embedded healthcare decision support system," *Decision Analytics Journal*, 2020.
- [19] M. Dua and D. Makhija, "A cnn-rnn-lstm based amalgamation for alzheimer's disease detection," *Journal of Medical and Biological Engineering*, 2020.
- [20] C. L. Saratxaga and I. Moya, "Mri deep learning-based solution for alzheimer's disease prediction," *Journal of Personalized Medicine*, 2020.
- [21] J. Liu and Y. Luo, "Alzheimer's disease detection using depthwise separable convolutional neural networks," 2020.
- [22] Urañinjo, "Augmented alzheimer mri dataset," <https://www.kaggle.com/datasets/uraninjo/augmented-alzheimer-mri-dataset/data>, 2024.
- [23] C. Szegedy, W. Liu, Y. Jia, P. Sermanet, S. Reed, D. Anguelov, D. Erhan, V. Vanhoucke, and A. Rabinovich, "Going deeper with convolutions," in *Proceedings of the IEEE conference on computer vision and pattern recognition*, 2015, pp. 1–9.
- [24] A. Vaswani, N. Shazeer, N. Parmar, J. Uszkoreit, L. Jones, A. N. Gomez, L. Kaiser, and I. Polosukhin, "Attention is all you need," *Advances in neural information processing systems*, vol. 30, 2017.
- [25] K. He, X. Zhang, S. Ren, and J. Sun, "Deep residual learning for image recognition," in *Proceedings of the IEEE conference on computer vision and pattern recognition*, 2016, pp. 770–778.
- [26] S. Woo, J. Park, J.-Y. Lee, and I. S. Kwon, "Cbam: Convolutional block attention module," in *Proceedings of the European conference on computer vision (ECCV)*, 2018, pp. 3–19.
- [27] G. Huang, Z. Liu, and K. Q. Weinberger, "Densely connected convolutional networks," *CoRR*, vol. abs/1608.06993, 2016. [Online]. Available: <http://arxiv.org/abs/1608.06993>
- [28] M. Tan and Q. V. Le, "Efficientnetv2: Smaller models and faster training," *CoRR*, vol. abs/2104.00298, 2021. [Online]. Available: <https://arxiv.org/abs/2104.00298>
- [29] C. Szegedy, S. Ioffe, and V. Vanhoucke, "Inception-v4, inception-resnet and the impact of residual connections on learning," *CoRR*, vol. abs/1602.07261, 2016. [Online]. Available: <http://arxiv.org/abs/1602.07261>
- [30] M. Sandler, A. G. Howard, M. Zhu, A. Zhmoginov, and L.-C. Chen, "Inverted residuals and linear bottlenecks: Mobile networks for classification, detection and segmentation," *CoRR*, vol. abs/1801.04381, 2018. [Online]. Available: <http://arxiv.org/abs/1801.04381>
- [31] A. G. Howard, M. Zhu, B. Chen, D. Kalenichenko, W. Wang, T. Weyand, M. Andreetto, and H. Adam, "Mobilenets: Efficient convolutional neural networks for mobile vision applications," *CoRR*, vol. abs/1704.04861, 2017. [Online]. Available: <http://arxiv.org/abs/1704.04861>
- [32] B. Zoph, V. Vasudevan, J. Shlens, and Q. V. Le, "Learning transferable architectures for scalable image recognition," *CoRR*, vol. abs/1707.07012, 2017. [Online]. Available: <http://arxiv.org/abs/1707.07012>
- [33] K. Simonyan and A. Zisserman, "Very deep convolutional networks for large-scale image recognition," *arXiv preprint arXiv:1409.1556*, 2015. [Online]. Available: <http://arxiv.org/abs/1409.1556>
- [34] F. Chollet, "Xception: Deep learning with depthwise separable convolutions," *CoRR*, vol. abs/1610.02357, 2016. [Online]. Available: <http://arxiv.org/abs/1610.02357>
- [35] S. Wang, Y. Zhang, Y. Li *et al.*, "Single slice based detection for alzheimer's disease via wavelet entropy and multilayer perceptron trained by biogeography-based optimization," *Multimedia Tools and Applications*, vol. 77, pp. 10 393–10 417, 2018.
- [36] S. Murugan, C. Venkatesan, M. G. Sumithra, X.-Z. Gao, B. Elakkiya, M. Akila, and S. Manoharan, "Demnet: A deep learning model for early diagnosis of alzheimer diseases and dementia from mr images," *IEEE Access*, vol. 9, pp. 90 319–90 329, 2021.

...